Physics Procedia

Volume 75, 2015, Pages 1271–1278

20th International Conference on Magnetism

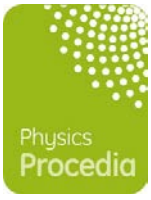

Enhancement of Sensitivity on Miniaturized Thin-film Magnetoimpedance with Ellipsoidal Element

Hiroaki Kikuchi[1*], Suguru Oe[1], Hiroaki Uetake[2], Shin Yabukami[2], Tomoo Nakai[3], Shuichiro Hashi[4] and Kazushi Ishiyama[4]

[1]*Iwate University, Morioka, Japan.*
[2]*Tohoku Gakuin University, Sendai, Japan.*
[3]*Industrial Technology Institute, Miyagi Prefectural Government, Sendai, Japan.*
[4]*Tohoku University, Sendai, Japan.*

Abstract

We tried to control the distribution of the demagnetizing field inside magnetoimpedance elements fabricated using thin-film to gain higher sensitivity. Elements with quasi-ellipsoidal shape were adopted to modify the demagnetizing field distribution, because it is well known that the demagnetizing field is expected to be uniform in an ellipsoid. The larger impedance change and higher sensitivity were obtained in the ellipsoidal elements compared to those of the conventional rectangular elements. The observed results were analyzed by the calculations on the basis of the distribution of the demagnetizing field and the impedance profile without demagnetizing effect. The calculations well explained the experimental results: the improvement of sensitivity and the performance for the ellipsoidal elements is attributed to the uniform distribution of demagnetizing field. The experimental results demonstrate a potential and the calculation results contribute to optimum design, for a miniaturization of magnetoimpedance element in order to keep the higher sensitivity.

Keywords: Magnetoimpedance, thin-film, demagnetizing field distribution, sensitivity

1 Introduction

Magnetoimpedance (MI) element utilizes rapid changes in an initial permeability when an external magnetic field is applied and also significant skin effect related to the permeability changes [Mohri, K. (1992)]. A MI element is typically designed to be applied with a small AC magnetic field parallel to the easy axis through high frequency current and to detect an external magnetic field parallel to the longitudinal direction of the element. Many fundamental researches have been extensively conducted on ribbons [Buznikov, N. (2004), Kraus, L. (2005)], wires [Chen, D. X. (1998), Vazquez, M. (1998),

* Corresponding author. Tel. +81-19-621-6890; fax: +81-19-621-6890
E-mail address: hkiku@iwate-u.ac.jp

Selection and peer-review under responsibility of the Scientific Programme Committee of ICM 2015

doi:10.1016/j.phpro.2015.12.141

Zhukova, V. (2002)], and thin-films [Panina, L. V. (1995), Xiao, S.Q. (1999)]; they were well reviewed and referred in [Phan, M-H. (2008)]. The MI element is commercialized as compasses in mobile phones [Cai, C. M. (2005)] and is also expected to be a highly sensitive magnetic field sensor for applications in various industrial fields: biological [Chiriac, H. (2005), Wang, T. (2014)], medical [Yabukami, S. (2009), Uchiyama, T. (2012)] field and nondestructive testing [Ozawa, T. (2013)]. On the other hand, demands for a miniaturization of MI elements increases on the miniaturization of electronic devices and in the detection with high spatial resolution. MI element fabricated using a thin-film gives a reply to the demands because the configuration is compatible with integrated electronic devices; thus the study of MI with thin-film increases recently [Garcia-Arribas, A. (2012), (2013), Fernandez, E. (2015)]. However, when a thin-film MI sensor is miniaturized, particularly its length becomes shorter, decrease in the sensitivity due to a demagnetizing field is ineludible. Previously, we revealed that the distribution of the demagnetizing field plays main role to deteriorate the sensing properties at the edge of the MI thin-film element [Kikuchi, H. (2015)]. The fact that a demagnetizing field becomes uniform in ellipsoidal ferromagnetic materials is well known and gives us a way to solve a fault related to demagnetizing effect. Thus, in this study, we fabricated MI thin-film elements with a quasi-ellipsoidal shape to conquer the disadvantage, i.e. to avoid the distribution of demagnetizing field in the elements. The impedance was measured and domain observations were experimentally performed and the results were compared to those of the conventional rectangular shaped elements; we investigated the usefulness of controlling the demagnetizing field distribution inside the elements to gain higher sensitivity on the miniaturized thin-film MI element. We also analyzed the obtained results by the estimation of impedance profile taking into account the distribution of the demagnetizing field.

2 Experimental Procedure

The amorphous $Co_{85}Zr_3Nb_{12}$ thin-films, used for the sensing elements, were deposited by a magnetron sputtering process. Then the films were shaped into ellipsoid or rectangle using a photolithography and lift-off processes. The elements were 20, 50, and 80 μm wide and 2 μm thick, and their total length was 1.4 mm (for the 20-μm-wide elements) and 1.7 mm (for the 50 and 80-μm-wide elements), respectively. The sensing part was 1 mm in all the elements. The shapes and the dimensions of the elements are shown in Fig. 1 (a) and (b). After fabricating the sensing elements, the elements were annealed at 673 K with an applied field of 3 kOe (240 kA/m) to adjust the direction of uniaxial anisotropy, i.e. the easy axis to be parallel to the width direction of the elements. Then, a 2-μm-thick Cu electrode was also fabricated by the same process as fabrication of sensing elements. The impedance of the sensing part was measured using a network analyzer (HP8752A) and a wafer probe (Picoprobe 40A-GSG-150-LP) by the reflection method with a 100 MHz AC current applied to the longitudinal direction of the elements (the small AC excitation field generated by the current, was

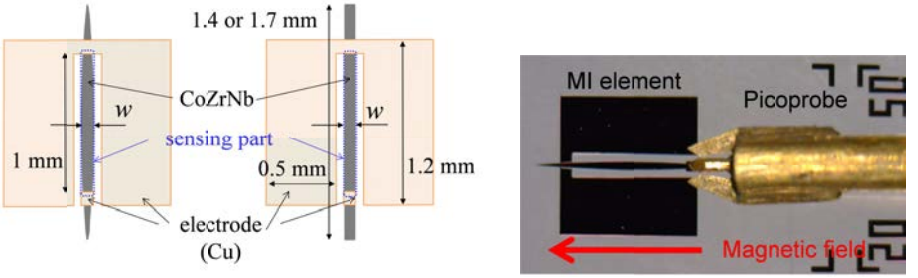

(a) ellipsoid (b) rectangle (c) view of measurement

Figure 1: Dimensions and shapes of fabricated thin-film element and view of measurement.

parallel to the width direction of the elements). The reasons why we used 100 MHz are that the skin effect becomes significant, and also the inductive effect is strongly remains around the frequency in the case of several μm thick. The photograph of the measurement is shown in Fig. 1 (c). The incident power to the elements was −20 dBm. A DC magnetic field was applied along the longitudinal direction of the elements by a Helmholtz coil during the impedance measurements and the domain observations.

3 Results

Figure 2 shows the changes in the absolute value of the impedance Z against the external DC magnetic field for both ellipsoid and rectangle with different width. The applied DC field changes from –20 Oe (–1.6 kA/m) to 20 Oe (1.6 kA/m). All the elements show the profile as follows: the impedance is minimum at $H = 0$ and takes two obvious peaks, which are typical MI profiles. The field intensity where the impedance becomes maximum, H_p, is about 8 – 10 Oe (0.64 – 0.8 kA/m), which is close to the anisotropy field H_k of the films. For example, the impedance is 39.3 Ω at $H = 0$, and it increases with increasing applied field, followed by taking 64.2 Ω at $H = 8.6$ Oe (0.69 kA/m) for the ellipsoidal element with 20-μm-wide. The characteristics obtained from the impedance profiles are summarized in Table 1. The value of ΔZ is defined as $Z_m - Z_0$, where Z_m is the maximum of the impedance, and Z_0 is the impedance at $H = 0$. The value of dZ/dH represents the maximum tangential slope of the impedance against magnetic field. The values of ΔZ, the impedance change ratio $\Delta Z/Z_0$, and dZ/dH for the ellipsoidal shape are larger than those for the rectangular shape in the same width. The obtained results can be explained qualitatively as follows: on the rectangular element, the demagnetizing field near the edge increases rapidly compared to the center parts, and the changing ratio of the demagnetizing field, is maxima at the end of the element, decreases toward center part and becomes constant. This distribution deteriorates rapid impedance changes, consequently the sensitivity

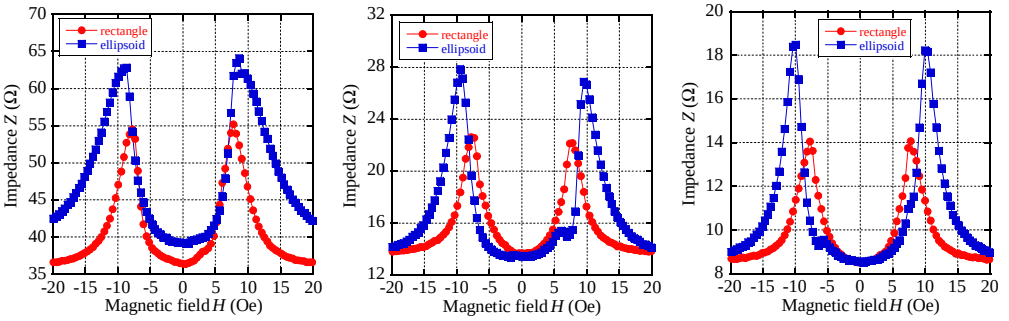

(a) 20 μm width (b) 50 μm width (c) 80 μm width

Figure 2: Impedance change against external magnetic field.

Table 1: Experimental values of ΔZ, $\Delta Z/Z_0$, dZ/dH and H_p in the ellipsoidal and rectangular elements.

width	shape	ΔZ (Ω)	$\Delta Z/Z_0$ (%)	dZ/dH (Ω/Oe)	H_p (Oe)
20 μm	ellipsoid	24.3	61.9	13.2	8.6
	rectangle	18.7	51.3	10.2	7.8
50 μm	ellipsoid	14.5	104.7	7.0	9.6
	rectangle	8.9	63.1	4.2	7.6
80 μm	ellipsoid	9.9	114.7	5.3	10.1
	rectangle	5.6	65.3	2.9	7.8

is modified. For ellipsoidal element, the demagnetizing field is expected to be uniform as compared with the rectangle, which is attributed to keeping higher sensitivity. More detailed and quantitative discussion will be done later. The values of ΔZ and dZ/dH increase with increasing width, which is because the sectional area of the element decreases. The value of H_p increases with increasing width, and H_p for the ellipsoid is larger than that for the rectangular element.

4 Discussions

Here, the impedance profiles, taking into account the distribution of the demagnetizing field in the elements, were calculated to analyze the observed experimental results. The calculation was done for both rectangular and ellipsoidal elements, and the dimensions for the calculations were the same as those of the experiments. At first we estimated the demagnetizing factor in the elements by the magnetic moment method (Qm, produced by Shift Lock Corporation). In the calculations, the longitudinal direction is defined as the x-axis and the center of the element is defined as the origin, x = 0. The magnetic flux density in the x-direction was calculated when a uniform magnetic field is applied to the longitudinal direction. The distribution of the magnetic flux density gives the demagnetizing factor N_x along x-axis. In this work, it is assumed that the demagnetizing factor N_x depends only on the configurations of the elements. The detailed calculation procedure appeared in [Kikuchi, H. (2015)]. Figure 3 plots the calculated demagnetizing factor N_x against the position x. The distribution for whole element is shown in Fig. 3 (a), and magnification of the sensing part ($-0.5 \leq x$ (mm) ≤ 0.5 in this work) is shown in Fig. 3 (b). We can see that the distribution of demagnetizing factor near the edge (x = –0.85, 0.85 for 50 and 80 µm-width-element, x = –0.7, 0.7 for 20 µm-width-element) rapidly increases on the rectangular elements (See Fig. 3 (a)). In the sensing part, the demagnetizing factor becomes relatively uniform in an ellipsoid compared to a rectangle, while the value of N_x for ellipsoid is larger than that for rectangle. The value of N_x depends on the position x; therefore, the demagnetizing field, H_{dem} (x) and the effective field in the element H_{eff} (x) become a function of position x as follows (in cgs units):

$$H_{eff}(x) = H_{ex} - H_{dem}(x) = H_{ex} - N_x(x)M(x) \quad (1)$$

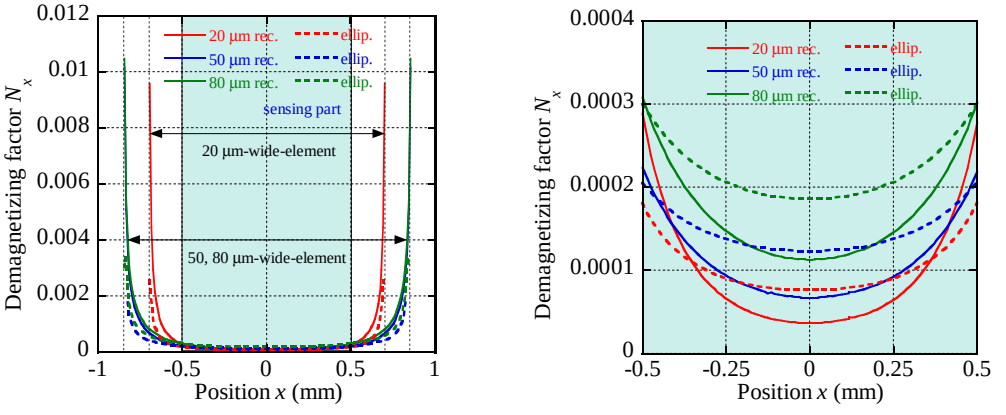

(a) whole element (b) enlarged sensing part

Figure 3: Dependence of the calculated demagnetizing factor on the position of the elements. The solid lines are the results for rectangle element and the dot lines for ellipsoid.

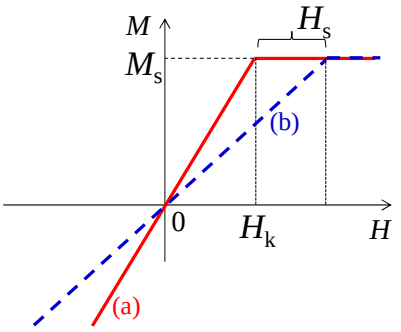

Figure 4: Delineation of the magnetization curves using calculations for the impedance profile that take into account the distribution of the demagnetizing field. (a) curve without demagnetizing (b) curve with demagnetizing.

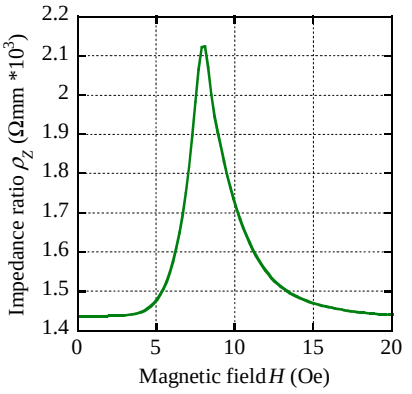

Figure 5: Impedance ratio ρ_z plotted against external magnetic field.

$$M(x) = \frac{M_s}{H_s + H_k} H_{ex} \tag{2}$$

$$H_s(x) = N_x(x) M_s \tag{3}$$

where H_{ex} is the applied uniform external field, M_s is the saturation magnetic flux density of the element, H_s is the demagnetizing field when the element is magnetically saturated. The magnetization curves for the calculation of $M(x)$ are shown in Fig. 4. The magnetization curve that does not consider the effect of demagnetizing field is represented as the curve (a) in Fig. 4, because the external field is applied to the longitudinal direction, i.e. the hard axis of the elements. The magnetization is proportional to the applied field up to anisotropy field H_k and then saturates. Considering the demagnetizing effect, additional field H_s, which is represented in equation (3), is required to magnetically saturate the material; hence the magnetization curve becomes the curve (b) in Fig. 4. When H_{ex} is altered, magnetization $M(x)$ is obtained by equation (2), and thus, demagnetizing field $H_{dem}(x)$ and effective field $H_{eff}(x)$ are obtained by equation (1).

In the present work, the width of the element depends on the position x for the ellipsoidal elements. Thus, we introduce the impedance ratio like resistivity as follows:

$$\rho_Z(H) = Z(H)\frac{wt}{l} \tag{4}$$

where, w, t, and l are width, thickness, and length of the element, respectively, and $Z(H)$ is the total impedance of the element and depends on the effective magnetic field.

Though l and t are constant in the experiments, w depends on the position x for the ellipsoidal elements, i.e., it becomes $w(x)$, while w is also constant for the rectangular elements.

Consequently, total impedance can be expressed:

$$Z(H) = \frac{1}{t}\int_{l_1}^{l_2} \frac{\rho_z\{H_{eff}(x)\}}{w(x)} dx \tag{5}$$

where l_1 and l_2 are the positions at the ends of the sensing parts of element. When the impedance ratio without demagnetizing field is given as $\rho_Z(H)$, the impedance profiles of the elements considering the effect of the demagnetizing field can be calculated. The function $\rho_Z(H)$ used in the calculation is given in Fig. 5. This profile is derived from our previous work [Kikuchi H. (2015)]. The parameters (l_1, l_2) are (–0.5, 0.5) for all the elements.

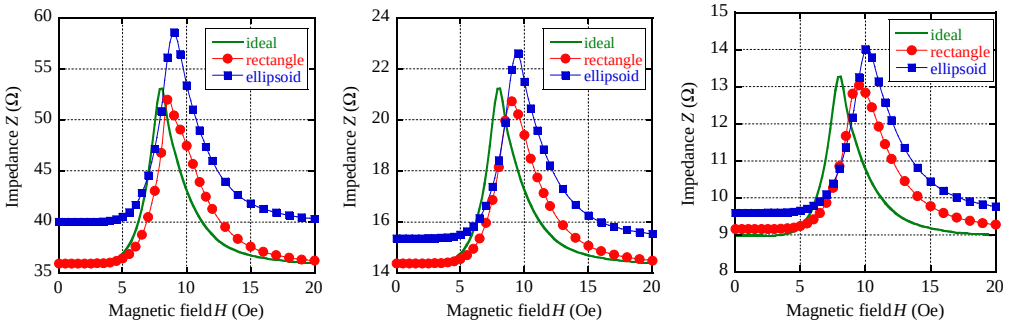

(a) 20 μm width (b) 50 μm width (c) 80 μm width

Figure 6: Calculated impedance profile that takes into account the distribution of the demagnetizing field. "ideal" means impedance profile without demagnetizing field. Dots show the estimated value calculated by equation (5) and functions $\rho_z(H)$ and $w(x)$.

Table 2: Calculated values of ΔZ, $\Delta Z/Z_0$, dZ/dH and H_p in the ellipsoidal and rectangular elements.

width	shape	ΔZ (Ω)	$\Delta Z/Z_0$ (%)	dZ/dH (Ω/Oe)	H_p (Oe)
20 μm	ellipsoid	18.6	46.4	9.0	9.0
	rectangle	16.1	44.7	8.9	8.5
50 μm	ellipsoid	7.2	47.1	4.0	9.5
	rectangle	6.3	44.1	3.6	9.0
80 μm	ellipsoid	4.4	45.9	2.2	10.0
	rectangle	3.9	42.4	2.3	9.5

Figure 6 plots the calculated impedance changes against the applied magnetic field. The green solid line is the ideal impedance profile without demagnetizing effect, and the red and blue dots show the results calculated with considering the demagnetizing effect. The same parameters as the experiments were obtained from the calculated impedance profiles and those parameters are summarized in Table 2. Although it is not clear on the impedance profiles, almost ΔZ, $\Delta Z/Z_0$, dZ/dH for ellipsoidal elements is larger than those for rectangular elements, which indicates that the ellipsoidal element is favorable to gain higher sensitivity and better performance. In the work, the sensing part is relatively far from the edge part, which is one of the reasons why the difference in sensitivity between the ellipsoid and rectangle is small. However, the calculated results show that the distribution of demagnetizing for ellipsoid is suppressed compared to the rectangle, which contributes to improve the sensitivity. On the contrary, though the distribution of demagnetizing field is improved on the ellipsoid, the strength of the demagnetizing field becomes large; this means the peak position shifts to higher field, which can be observed on both calculated and experimental results. We see that there is a qualitative good agreement between the experimental and the calculated results, while some quantitative differences exist between them. The differences may be mainly attributed to local variations of the magnetic properties including both angle and strength dispersions of anisotropy within the substrate in which all the elements tested here were fabricated (26 mm square in the present work).

The evidence of the distribution of demagnetizing field was confirmed by the domain observations with a Kerr - effect microscope. Figure 7 shows the images of domain observation for 80-μm-wide elements. We can see that 180° domain propagates in the rectangular element, whereas the multiple domains appear and disappear from or to single domain simultaneously everywhere in the ellipsoidal element; these behaviors are attributed to the distribution of the demagnetizing field.

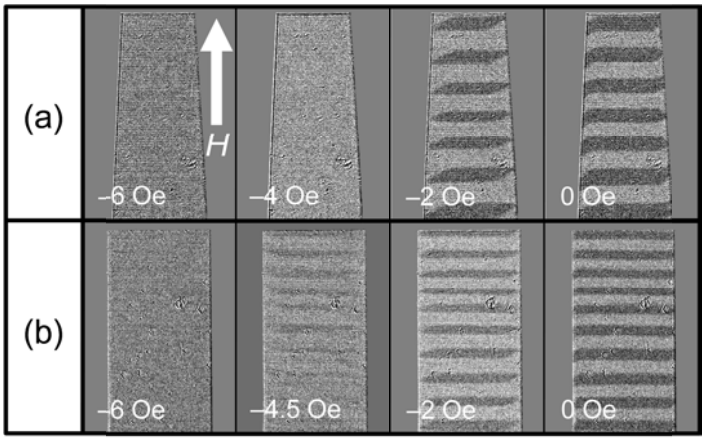

Figure 7: Domain observations for the 80-μm-wide elements: (a) ellipsoid; (b) rectangle.

5 Conclusions

To improve the sensitivity and the performance of miniaturized MI thin-film element, the ellipsoidal elements were fabricated and the properties have been investigated as compared with the conventional rectangular element. Large impedance changes and higher sensitivity were observed in the ellipsoidal elements; they are attributed to the suppression of the distribution of the demagnetizing field. The obtained results were confirmed by the calculations on the basis of the distribution of the demagnetizing field and the impedance profile without demagnetizing effect. Our experimental results indicate a potential of a miniaturized MI element with higher sensitivity and the calculations provide a guide for optimum design leading to the development of a higher-sensitivity magnetic field sensor with small dimensions.

Acknowledgement

This work was supported in part by the Cooperative Research Project of the Research Institute of Electrical Communication, Tohoku University, and in part by the Grant-in-Aid for Scientific Research (B), Grant No. 25289119, from the Japan Society for the Promotion of Science.

References

Mohri, K., et al., (1992). *IEEE Trans. Magn.*, 28, pp. 3150–3152.
Buznikov, N. A., et al. (2004). *Appl. Phys. Lett.*, 85, pp. 3507–3509.
Kraus, L., et al., (2005). *J. Magn. Magn. Mater.*, 290-291, pp. 1131–1133.
Chen, D. X., et al. (1998). *Phys. Rev.* B, 57, pp. 10699–10704.
Vazquez, M., et al., (1998). *IEEE Trans. Magn.*, 34, pp. 724–728.
Zhukova, V., et al., (2002). *J. Magn. Magn. Mater.*, 249, pp. 79–84.
Panina, L. V., et al., (1995). *IEEE Trans. Magn.*, 31, pp. 1249–1260.
Xiao, S.Q., et al., (1999). *J. Appl. Phys.*, 85, pp. 4127–4130.

Garcia-Arribas, A. et al., (2012). *IEEE Trans. Magn.*, 48, pp. 1601-1604.
Garcia-Arribas, A. et al., (2013). *Eur. Phys. J.* B, 86, 136.
Fernandez, E., et al., (2015). *IEEE Trans. Magn.*, 51, 6100404.
Phan, M-H., Peng H-X., (2008). *Prog. Mater. Sci.*, 53, pp. 323–420.
Cai, C. M., et al., (2005). IEEE International Magnetics Conference, 2005, pp. 407–408.
Chiriac, H., et al., (2005). *J. Magn. Magn. Mater.*, 293, pp. 671–676.
Wang, T., et al., (2014). *Biosens. Bioelectron.*, 58, pp. 338–344.
Yabukami, S., et al., (2009). *J. Magn. Magn. Mater.*, 321, pp. 675–678.
Uchiyama, T., et al., (2012). *IEEE Trans. Magn.*, 48, pp. 3833–3839.
Ozawa, T., et al., (2013). *J. Magn. Soc. Jpn.*, 37, pp. 1–7.
Kikuchi, H., et al., (2015). *Sens. Acuta.* A, 230, pp. 142–149.